DOI: 10.1002/psc.3305

RESEARCH ARTICLE



The impact of thermal history on the structure of glycylalanylglycine ethanol/water gels

Lavenia J. Thursch¹ | Thamires A. Lima¹ | Reinhard Schweitzer-Stenner² | Nicolas J. Alvarez¹

Correspondence

Reinhard Schweitzer-Stenner, Department of Chemistry, Drexel University, Philadelphia, PA 19104, USA.

Email: rschweitzer-stenner@drexel.edu

Nicolas J. Alvarez, Department of Chemical and Biological Engineering, Drexel University, Philadelphia, PA 19104, USA. Email: nja49@drexel.edu

Funding information

National Science Foundation (USA), Grant/ Award Number: DMR-1707770 This work revisits several open questions regarding the mechanisms of GAG fibril formation and structure as a function of temperature. The authors recently hypothesized that there is a solubility limit of GAG in ethanol/water that induces self-assembly. In other words, not all peptides can participate in fibrillization and some fraction is still soluble in solution. We show via FTIR spectroscopy that, indeed, free peptides are still present in solution after fibril formation, strongly supporting the solubility model. Furthermore, previous work showed GAG self-assembled into right-handed (phase I) or left-handed (phase II) chiral structures depending on temperature. In this study, we analyze the crystalline structure of phase I and II gels via WAXS and SAXS to compare their crystalline structures and order. Rheological measurements were used to investigate the response of the fibrillar network to temperature. They reveal that the ability of the peptide to self-assemble depends on the solubility at a given temperature and not on thermal history. Furthermore, the gel softening point, the linear viscoelastic gel microstructure, and relaxation spectrum are very similar between phase I and phase II. Overall, the temperature only affects the chirality of the fibrils and the formation kinetics.

1 | INTRODUCTION

Small molecules that form gels in water, hydrogels, and organic solvent, organogels, are known as low molecular weight gelators (LMWG). An emerging class of LMWG are small peptides with the propensity to form nano- and micro-fibrils that entangle into volume spanning networks. One major motivation for the study of peptide self-assembly is their relation to the formation of amyloid fibrils, which has been implicated in several disorders, such as Parkinson's disease, Huntington's disease, and so-called polyalanine diseases.^{1–3} Moreover, peptide fibril hydrogels are of interest for biomedical applications due to their high biocompatibility, tunable chemistry to control structure-properties relationships, and adaptability to environmental conditions.^{4–8} Biomedical applications for LMWG peptides include cell encapsulation,^{9–11} tissue engineering,^{12,13} and drug delivery.^{14–16}

Peptide residues with the highest propensity for self-assembly in water are hydrophobic aromatic amino acids. ^{17,18} However, several peptides without aromaticity have been shown to readily self-

assemble into fibril networks. For example, glycine-alanine-glycine (GAG) and glycine-histidine-glycine (GHG) self-assemble into very long microfibrils under the right conditions. ^{19–26} More specifically, GAG forms fibrils in the presence of a critical fraction of ethanol that depends on peptide concentration. ²⁶ While GHG forms fibrils when the pH of the solution exceeds the pKa of the imidazole side chain. ²¹

Recent experimental studies suggest the hypothesis that GAG's self-assembly is initiated by the accumulation of GAG at the ethanol/water interface, with the protonated C-terminal immersed in ethanol and the N-terminal exposed to water. ¹⁹ The amide I' region of the GAG fibrils exhibits a doublet with rather sharp bands at 1644 and 1670 cm $^{-1}$, which means that GAG does not self-assemble into typical β -sheet tapes or ribbons. ¹⁹ Note that β -sheets are generally considered the fundamental building block of amyloid-like fibrils. ^{27,28} Furthermore, the enhanced VCD signal of the amide I' mode reveals that the chirality of the peptide fibrils depends on the self-assembly temperature. ²³ Fibrils with a right-handed helical twist form below 15°C (phase I), whereas fibrils with a left-handed twist form above 16°C (phase II).

¹Department of Chemical and Biological Engineering, Drexel University, Philadelphia, PA, USA

²Department of Chemistry, Drexel University, Philadelphia, PA, USA

The strength and kinetics of GAG gels were measured via small amplitude oscillatory shear (SAOS) rheology. The storage moduli of GAG gels are considerably high for LMWG and depending on peptide concentration can range from 10³ to 10⁵ Pa.²³ The rate of gel formation depends strongly on the fraction of ethanol and peptide concentration and the optimum gel strength occurs at intermediate rates.²⁶ The modulus of phase I GAG fibril networks are higher than phase II, but a detailed study regarding the differences of these two phases has not been presented until now.

Previous studies on GAG suggest that the fibrils represent a meta-stable state and that an equilibrium state can only be obtained at higher temperature.²¹ For example, a linear viscoelastic temperature sweep revealed that the modulus is a continuous function of temperature. Microscopic imaging showed that the number of fibrils decreases with increasing temperature, and the storage modulus is proportional to the number of fibrils. Annealing the sample at 50°C followed by quenching at 5°C and 20°C showed a delay in the onset of gelation and a decrease in the overall modulus. Note that fibrils did not reform upon cooling after annealing for 16 h at 50°C.²¹ However, spectroscopic analysis of the sample revealed that the solution still contained peptide oligomers. Interestingly, phase I gels (formed at 5°C) showed both faster formation kinetics and better recovery of the elastic modulus (G') after several annealing cycles compared to phase II gels (formed at 20°C). Taken together, the results of these experiments suggest that in both phases, the gel is in a kinetically arrested, metastable state.

The authors recently hypothesized that the solubility of GAG in ethanol/water mixtures controls the rate of fibril formation and gel strength. More specifically, at high ethanol fractions and/or peptide concentrations, GAG is less soluble and more readily self-assembles into fibrils, denoted by faster gel kinetics. Annealing at higher temperatures, induces the formtaion of stable oligomers with increased solubility in the ethanol solution. For our solubility hypothesis to hold, it must also explain the reported differences between phase I and phase II fibril networks. Furthermore, the reformation kinetics should also be explainable in this framework. This paper uses spectroscopy, X-ray scattering, and rheology to test the solubility model on the observed phenomena of phase I and phase II fibril gels. We find that the data are in strong support of the solubility model, especially considering the metastable state of the fibrils.

2 | MATERIALS AND METHODS

2.1 | Materials

Unblocked glycyl-alanyl-glycine (H-Gly-Ala-Gly-OH) was purchased from Bachem with >99% purity and used without further purification. The gel samples were prepared by mixing the as-received peptide powder in a solvent phase constituted of 55 mol% ethanol (200 proof, Pharmco-Aaper) and 45 mol% deionized water. Hydrochloric acid (ACS grade, Ricca Chemical Company) was added to the solutions to ensure complete protonation of GAG. Deuterated solvents, D₂O

(99.9% purity, Sigma Aldrich) and ethan (ol)-d (EtOD, 99.9% purity, Sigma Aldrich), were used for Fourier transform infrared spectroscopy (FT-IR) experiments to avoid the overlap of the strong water band at $1640~\rm cm^{-1}$ with the amide I region ($1600-1700~\rm cm^{-1}$). EtOD is the deuterated ethyl alcohol with the alcoholic hydrogen replaced by deuterium. The protocol for the gel preparation was described in detail in earlier publications.

2.2 | Vibrational spectroscopy

FT-IR experiments were carried out using a Thermo Nicolet Nexus 870 FT-IR spectrometer in absorbance mode. Spectra were recorded with 32 scans at a 4 cm⁻¹ resolution at room temperature with a deuterated triglycine sulfate (DTGS) detector in 650-4000 cm⁻¹ range for mid-infrared (M-IR) spectra. The gels were prepared as previously described. We let the gel network develop for 2 h, which according to rheology is after steady state, and then a spatula was used to squeeze the samples to separate the fibrils and supernatant parts of the gels.

2.3 | Wide-angle X-ray scattering

The wide-angle X-ray scattering (WAXS) experiments were carried out on a Xenocs Xeuss 2.0 diffractometer operated at a voltage of 50 kV and a current of 0.6 mA equipped with a Cu K α X-ray source (Xenocs Genix^{3D} Cu ULD) with a 1.54 Å wavelength. A Dectris Pilatus 1M solid state detector was used. The distance between the sample and detector was 165 mm. A set of slits controlled the beam focal spot which was adjusted to 0.7 mm \times 0.7 mm. The samples were placed between two Kapton® windows in a cell mounted onto an X–Z scanning motor. An initial scan was run to find the minimum transmitted intensity that corresponds to the highest density of material. Each sample was exposed for 10 min. The obtained 2D diffraction patterns were analyzed using the Foxtrot software.²⁹ A silver behenate sample was used to calibrate the measurements.

2.4 | Small-angle X-ray scattering

The experiment was carried out using a Rigaku SMAX 3000 X-ray diffractometer. The X-ray source was a MicroMax-002 sealed tube operated at a voltage of 40 kV and a current of 88 mA. The beam focal spot was 20 mm \times 20 mm and the generated radiation was $CuK\alpha$ at a 1.54-Å wavelength. The samples were mounted on a plate placed onto an X-Y scanning motor. The 2D diffraction patterns were analyzed using the Datasqueeze software. A silver behenate sample was used to calibrate the measurements. The signal was then integrated over a 90° angle with the 0° aligned along the longest feature, in the case of the gel. The scattering vector $(q = \frac{4\pi \sin \theta}{\lambda})$ (1) from 0 to 0.22 Å⁻¹ was plotted against the angle and fit to a polynomial function.

2.5 | Scanning electron microscopy

Scanning electron microscopy (SEM) images were taken with a Zeiss Supra 50 VP instrument. Because the instrument operates under vacuum, the samples were prepared as described above and then dried before observation. Platinum was sputtered onto the dried samples to increase the sample conductivity and minimize artefacts.

2.6 | Rheology

Rheology measurements were obtained on a DHR-3 rheometer (TA instruments) using a Peltier plate for temperature control with a top plate of diameter 25 mm. Around 400 μ l of peptide material was used. A gap of 700 µm was applied. To avoid solvent evaporation, safflower oil was added as a solvent trap around the free surface of the sample. The ethanol/water solutions were confirmed to have little to no solubility in the oil phase. All samples were prepared 1 to 3 min prior to loading. The exact time between ethanol addition and beginning of the experiment was recorded and accounted for during data treatment. The mechanical properties of the hydrogel were probed by small amplitude oscillatory shear (SAOS) measurements. To monitor the initial gelation at either 5°C or 20°C, the storage modulus was measured versus time over a period of 5800 s by applying a strain of 0.03%, and an angular frequency of 1 rad s⁻¹. The sample was then brought to 50°C at a rate of 15°C per min, held at 50°C for 5 min, brought back to 5°C or 20°C at a rate 15°C/min and then incubated for 5800 s while recording modulus. We obtained this way two kinds of gels: as formed (before melting) or reformed (after melting and subsequent cooling). Both types of materials were further investigated with (1) a frequency sweep carried out between 0.02 rad s⁻¹ and 100 rad s⁻¹ at a constant 0.03% strain, and (2) a slow temperature ramping of 0.25°C/min to obtain the melting curves of the gels. We characterized these curves by graphically determining a softening point which coincides with the observed "knee." To find the precise value, the initial modulus plateau, as well as the region of sharp modulus decrease, was fit by exponential functions (since the traces are linear on a semi-log y plot). The softening temperature is defined as the intersection of the two lines.

3 | RESULTS AND DISCUSSION

3.1 | FTIR spectroscopy

FTIR spectroscopy allows us to investigate the state of the peptide fibrils and whether there are peptide molecules present in the liquid phase after fibrillization. Figure 1 presents the FTIR amide I region (1600–1700 $\rm cm^{-1}$) of pure GAG powder, fibrils, and supernatant for gel phases I and II formed from a 220-mM GAG in a 55-mol % ethanol/D₂O solution. The full spectrum from 0 to 3500 $\rm cm^{-1}$ is available in Figure S1.

The powder and fibril spectra show a sharp split of the amide I profile into bands at 1644 cm $^{-1}$ (Al₁) and 1673 cm $^{-1}$ (Al₂). For the

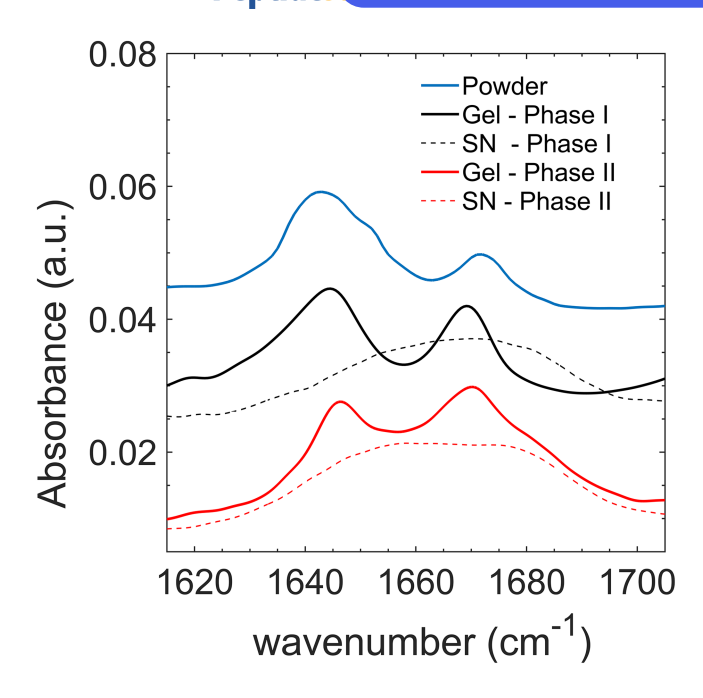


FIGURE 1 FTIR spectra of precipitated GAG (blue), phase I (black), and phase II (red) fibrils (line) and supernatant (dashes) samples from the 220-mM GAG gel. The spectra were vertically shifted for clarity

peptide powder, the peak intensity for Al_1 is twice that of the Al_2 peak intensity, which indicates substantial excitonic coupling between individual amide I modes and thus a rather high degree of molecular order.³¹ The fibrils' spectrum shows a qualitatively similar doublet but a reduced peak intensity ratio (i.e., $Al_1/Al_2 = 1.2$ for phase I and slightly below 1 for phase II).

The supernatant data show only a single amide I profile composed of two broad overlapping amide I' bands similar to observations for sol phase GAG in water/ethanol with ethanol fractions above 40 mol% ethanol as well as for GAG/water/ethanol mixtures after long annealing times. Thus, the supernatant is likely to be comprised of monomers and small amorphous oligomers.

These results strongly support the solubility hypothesis, that is, only a fraction of peptides participate in fibrillization and that a sol-like fraction remains in solution. Furthermore, the ratio between phase I and II areas of amide I bands, normalized by the intensity of the EtOD peak (1923 cm⁻¹), indicates that phase II presents twice as many peptides dispersed in the supernatant than phase I, suggesting that more peptides self-assemble into fibrils in phase I compared to phase II. More experiments are underway to quantitatively confirm these findings. Furthermore, this result explains the relatively higher modulus of phase I gels, compared to phase II gels, when measured at the formation temperature.²¹

3.2 | Wide-angle X-ray scattering

A systematic study of crystalline structure of GAG fibrils has not been presented to date. WAXS measurements were conducted to

investigate the differences in crystalline structure of phase I and phase II gels. Previous results showed that phase I gels recover to a higher modulus after thermal annealing compared to phase II gels. This suggests that there might be differences in crystalline structure of the two gel states. Furthermore, it is interesting to compare the crystalline structure of the gel states to the as-received precipitated peptide powder.

In the case of the as-received precipitated peptide, the diffraction pattern shows discrete intense rings indicating a crystalline structure (see Figure S2a). The diffraction patterns of the two gels show attenuated rings, with an amorphous background that is characteristic of solvent (see Figure S2b). The 2D patterns were integrated over the azimuthal angle 2π to generate intensity versus q plots. The amorphous background was determined by fitting a Gaussian function (see Figure S3) and subtracted from the experimental data. The intensities were normalized by the peak intensity at $q = 1.83 \text{ Å}^{-1}$. Figure S4 shows that the methodology applied to two distinct phase II gel samples results in identical peak distributions, and relative peak intensities. This confirms the reproducibility of the crystalline structure and validates our pattern analysis methods.

Figure 2 compares the WAXS signal of the precipitated peptide with phase I and phase II gels formed from a 200-mM GAG 55-mol% ethanol/ H_2O solution at 5°C and 20°C, respectively. Typical of powder diffraction patterns, many crystalline peaks are observed. Surprisingly, we observe very similar peak positions between phase I and phase II gels, indicating very similar, if not exact, crystalline unit cell structure. There are some quantitative differences between relative peak heights, for example, at $q = 1.77 \, \text{Å}^{-1}$ and $1.83 \, \text{Å}^{-1}$. On the contrary, the diffraction pattern of the precipitated peptide shows a very distinct crystalline structure compared to the two gel phases. These results clearly indicate that the crystalline fibrils formed in the presence of ethanol are fundamentally different than the crystals formed by precipitation. This observation is consistent with the hypothesis that the peptides organize at the ethanol/water interface,

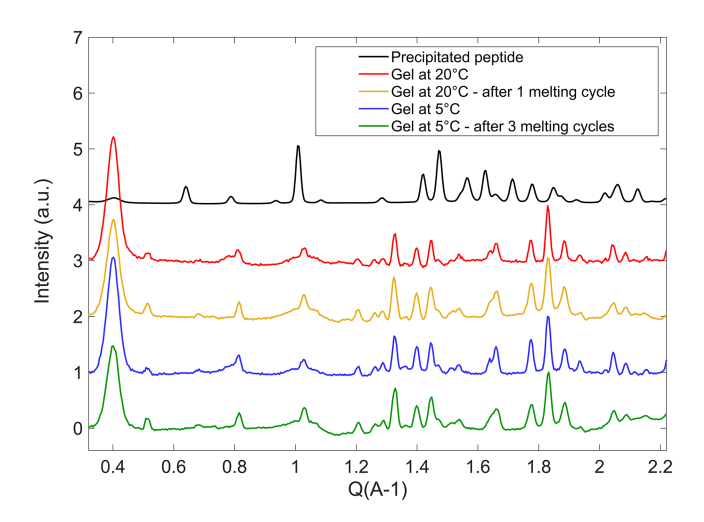


FIGURE 2 Wide-angle X-ray scattering spectra of precipitated peptide and gel with 220-mM GAG formed at 5° C and 20° C and after melting at 50° C and reformation at 5° C and 20° C

which favors a different interaction potential and a unique selfassembled structure.

Although spectroscopic measurements do not indicate the formation of a canonical β -sheet, we do observe scattering peaks characteristic of β -sheet distances. Following the Bragg condition, the $1.2\,\text{Å}^{-1}$ peak corresponds to $5.2\,5.2\,\text{Å}\,(n=1)$ or $10.5\,\text{Å}\,(n=2)$ in real space. This is consistent with expected distances between strands of a β -sheet or between β -sheets in stacks, respectively. This does not necessarily mean that the fibrils form β -sheets, similar distances can be expected for alternative arrangements. 31

We have previously shown that the kinetics and VCD signal of the reformed phase I and phase II crystals after annealing at 50°C are slower, whereas the original chiralities of these phases are maintained.²¹ Furthermore, rheology recorded after three annealing cycles at 50°C of a phase I gel showed a significant loss of rigidity as measured by the storage modulus. Figure 2 depicts 1D WAXS patterns of phase II and phase I fibrils after one and three annealing cycles, respectively. There is no notable difference in the crystalline structure before or after annealing. This strongly supports the hypothesis that annealing at 50°C decreases the number of peptides that form fibrils and subsequently decreases the number of fibrils in the network. However, the crystalline structure and chirality are unchanged and depend only on the fibril formation temperature.

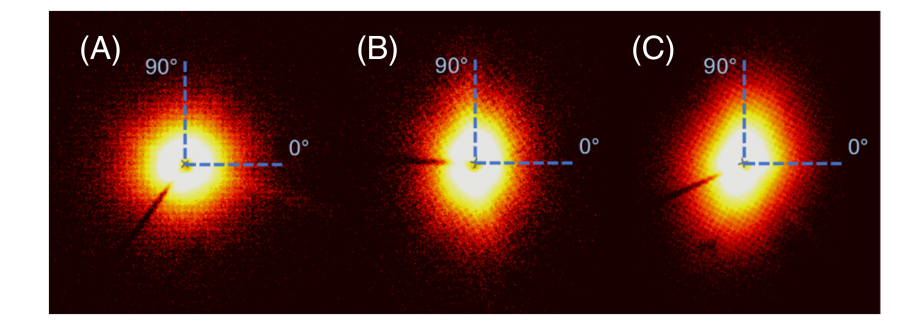
3.3 | Small-angle X-ray scattering

Figure 3 shows the 2D SAXS patterns for precipitated peptide powder, phase I, and phase II gels. As expected, the precipitated powder shows a random distribution of crystalline domains, denoted by the isotropic scattering pattern. The phase I and phase II gels show a preferential scattering in one direction, which is indicated by the asymmetric scattering pattern. This is coherent with the SEM images of the gels that show preferential alignment of the fibrils in one direction (see Figure 4). We used the Herman's orientation function to quantify the overall alignment in each 2D pattern. The function calculates a parameter f which ranges between -0.5 and 1, where unity indicates perfect alignment along the 90° axis and -0.5 indicates perfect alignment along the 90° axis. The Herman's orientation factors were calculated according to the formula:

$$f = \frac{3\left(\cos^2(\phi)\right) - 1}{2} \operatorname{with}\left(\cos^2(\phi)\right) = \frac{\int_0^{\frac{\pi}{2}} I(\phi) \sin(\phi) \cos^2(\phi) d\phi}{\int_0^{\frac{\pi}{2}} I(\phi) \sin(\phi) d\phi}, \quad (1)$$

where I is the relative intensity at a scattering angle Φ . For the precipitate peptide, f is close to zero, f = 0.009, which indicates an isotropic distribution of powder. On the other hand, the phase I and II fibril networks show a degree of preferential alignment.³³ The Herman factors for the two gel samples are comparable at -0.206 and -0.222 for 5° C and 20° C, respectively. The preferential alignment can explain to some degree the high packing efficiency of the fibrils to form strong networks with large moduli. Combined with the WAXS data above, phase I and II fibrils do not have different crystalline

FIGURE 3 Small-angle X-ray scattering patterns of (A) precipitated peptide, (B,C) gels with 200-mM GAG obtained at 23°C and 5°C, respectively



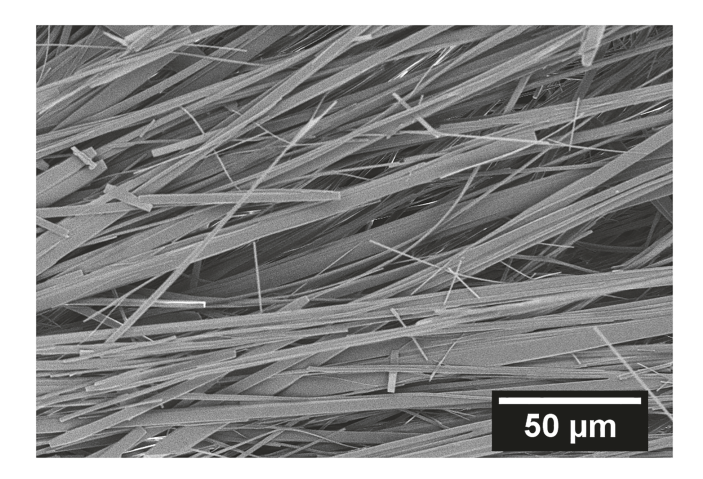


FIGURE 4 SEM capture showing the microscopic structure of the GAG network

structures or packing/orientation. Hence, the only structural difference between phase I and II fibrils is their chirality probed by their amide I VCD signal, which indicates left and right-handed chirality depending on formation temperature.

3.4 | Rheology

We now revisit the rheological response of phase I and II gels to test the solubility hypothesis presented by Thursch et al. ²⁶ Figure 5 shows the formation kinetics via storage modulus as a function of time for phase I and II gels for different thermal histories. As reported earlier, the sample formed at 5°C shows a higher modulus than the sample formed at 20°C, and this difference is more pronounced for relatively low GAG concentrations (150 mM). We argue that the higher modulus is caused by the formation of more fibrils at lower temperature. In other words, GAG monomers are less soluble at lower temperatures and therefore more peptides form more fibrils. This was confirmed by circular dichroism experiments showing that the signal characteristic of fibrils at 221 nm is correlated to the storage modulus of the gel sample. ²²

We have previously shown that annealing phase II gel networks at 50°C induces a transition of the GAG monomer into a state that is no longer capable of forming fibrils. For example, the CD signal after 16 h of annealing at 50°C shows that that the positive maximum of

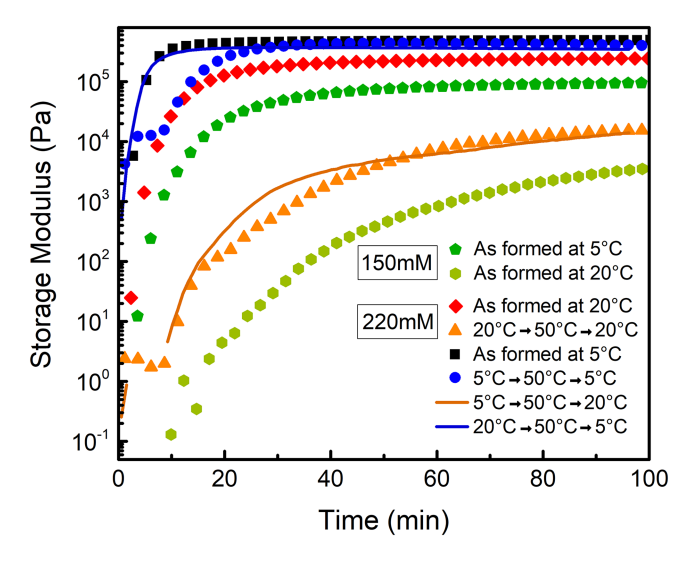


FIGURE 5 Time dependence of the storage modulus of gel samples as formed at 5°C or 20°C and with 1 melting cycle at 50°C and reformation at 20°C or 5°C. The GAG concentrations presented are 150 and 220 mM

the latter at 220 nm is replaced by a negative minimum, which suggests the absence of fibrils. ²¹ However, phase I and II gels showed identical signals after 16 h of annealing. We are interested in quantifying the gel strength after shorter exposure to elevated temperatures. The phase I and phase II fibril gel samples were annealed at 50°C for 5 min and cooled back down to their respective formation temperatures. Figure 5 shows the reformation kinetics of several gel samples for comparison. The modulus reformation kinetics for 20°C is considerably slower than the initial formation and plateaus at a significantly lower storage modulus. The reformation kinetics for 5°C shows slower dynamics compared to the original formation but produces only a slightly lower modulus. These results signify that after only 5 min, regardless of formation temperature, there is a decrease in the number of peptides participating in fibrillization.

The significant difference in reformation modulus between phase I and phase II gels can be explained by the fact that modulus is not a linear function of the number of fibrils. We have shown previously that above a critical fraction of fibrils, the modulus is a very weak function of fibril density.²¹ From elasticity theory, the modulus is inversely proportional to the average distance between entanglements, where entanglements here are defined as the physical

overlapping of fibrils, that is, friction points. Our results imply that above a critical fraction, new fibril formation only slightly decreases the average distance between physical entanglements between fibrils. If we assume that the same number of peptide monomers were converted to soluble oligomers during annealing, the only conclusion is that the solubility of GAG monomer is significantly lower at 5°C than 20°C, forming significantly more fibrils from the same available GAG monomer.

The assumption that the same number of peptide monomers are converted to a stable soluble oligomer, regardless of formation temperature, is supported by Figure 5. More specifically, the transient elastic modulus is compared for a phase I fibril network reformed at 20°C (represented by an orange line) and a phase II fibril network reformed at 20°C (represented with orange triangles). Regardless of the starting state of the fibrils, the same kinetics and modulus are observed after thermal annealing. In other words, the fraction of peptide monomer converted to the stable state is independent of initial formation temperature.

An interesting discussion point is the thermal stability of phase I and phase II fibrils. Figure 6 shows the temperature sweep of a phase I and II fibril network with different thermal histories. As discussed previously, the modulus is a continuous decreasing function of temperature, which supports the notion that there is a steady state number of self-assembled peptides that are decreasing with increasing temperature for both phase I and II gels. However, if the thermal equilibrium did not depend on the type of fibril, then one would expect that the temperature sweep of a phase I and II gel would superimpose. Figure 6 clearly shows that the curves do not superimpose. In fact, phase II gels show a slightly higher thermal stability compared to phase I gels, irrespective of starting peptide concentration or thermal history. The increased stability of phase II gels is denoted by the weak dependence of modulus on temperature from

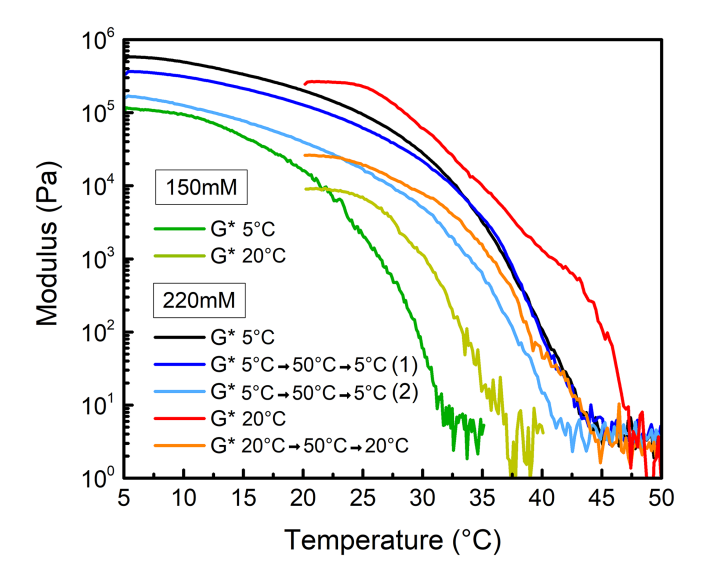


FIGURE 6 Complex modulus as a function of temperature of gel samples with 150 or 220 mM GAG, as formed or after one (1) or two (2) melting cycles

 $20^{\circ}\text{C}-30^{\circ}\text{C}$, and the higher temperature required to achieve the same modulus as phase I gels. This suggests that the solubility of phase II fibrils is slightly lower than phase I fibrils.

This observation is consistent with previous observations of Farrell et al., who probed the melting of the above gel phases with UV circular dichroism (CD) spectroscopy. They reported melting temperatures of 302 and 310 K for phase I and II gels, respectively.²³ As argued by DiGuiseppi et al.,21 the specific CD spectrum of GAG gel phases reflect the degree of peptide fibrilization. The dichroism value measured at 221 nm is more pronounced at the respective formation temperature for phase I compared to phase II, indicating a larger number of fibrils in phase I. A thermodynamic analysis of the CD-based melting curve in terms of a two-state model revealed that enthalpic contributions stabilize phase II to a significantly larger extent than phase I (241 versus 141 kJ mol⁻¹). This discrepancy is only partially compensated by the negative entropy changes associated with the formation of the two phases (0.77 and 0.47 kJ mol^{-1} K). These results suggest that the fibrils formed in phase II are energetically more stable. It is yet unclear how this result can be related to the observation of very similar crystalline structures.

In previous studies, we have focused only on the modulus at a given frequency. However, it is interesting to consider the full frequency spectrum of the linear viscoelastic envelop for the different phase fibril networks. Figure 7A,B shows the linear viscoelasticity of phase I and II fibril networks with different thermal history. For the two gel phases and the two concentrations, the storage moduli G' increases with frequency and exceeds the low modulus for the entire frequency range studied. The phase angle simultaneously decreases, suggesting frictional losses are occurring over long timescales. This signifies that the fibril networks are restructuring on timescales above 100 s. The phase II fibril network (20°C) displays the closest moduli at 0.02 rad/s. We plotted the ratio $\tan \delta = \frac{G''}{G'}$ in Figure 7C to help visualize the viscoelastic effects. Phase II networks exhibit a higher tan δ for most of the range compared to phase I. This signifies that phase II gels have more mobility than phase I gels. After thermal annealing, the phase II fibril network shows a much smaller $tan\delta$ at higher frequency, indicating that the network is more homogeneous with less mobility. This supports the observation that slower kinetics lead to more homogeneous networks.²⁶

A common tool in colloidal rheology is to compare the relaxation distribution of colloidal networks. The G' and G'' frequency sweep data in Figure 7A,B can be discretized into a discrete relaxation spectrum, $G(\tau)$, where g_i and τ_i are the modulus and timescale of relaxation mode i. Note that only two modes per decade were used. The relaxation-time distribution, $H(\tau)$, was calculated using the following formula,

$$H(\tau) = \sum_{i=0}^{N} g_i \delta\left(1 - \frac{\tau}{\tau_i}\right), \tag{2}$$

where δ is the Dirac function. For colloidal gels, Zaccone et al. described two aggregation mechanisms based on the functional form of $H(\tau)$: diffusion-limited and kinetic-limited aggregation. The power-law dependence of $H(\tau)$ at low frequency indicates the dominating

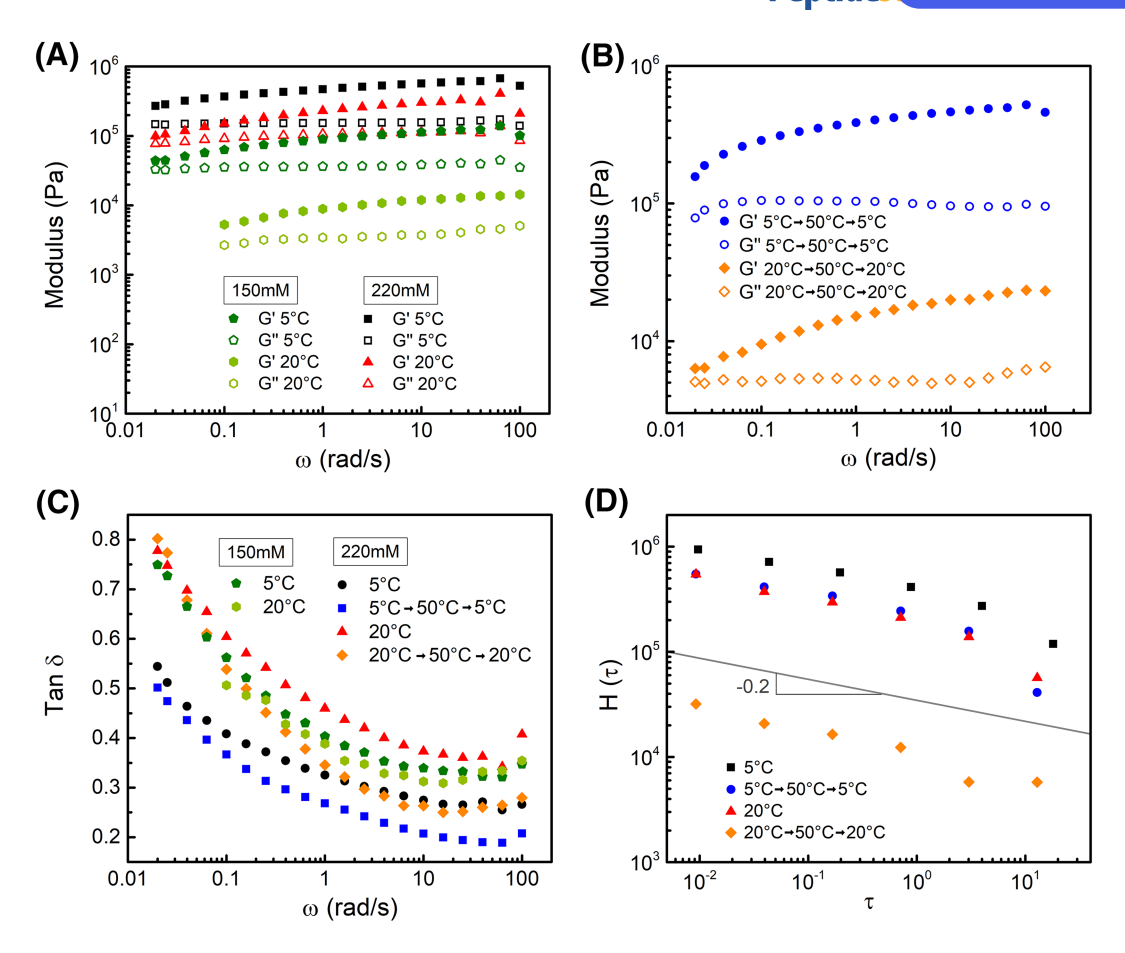


FIGURE 7 Frequency dependence of the storage and loss moduli of gel samples with 150 or 220 mM GAG, (A) formed at 20°C and 5°C, (B) with a melting cycle at 50°C and reformation at 5°C and 20°C, (C) tan δ of all gel samples, (D) relaxation time spectra calculated from the frequency sweeps

mechanism. A slope n = -0.5 indicates the limit of reversible kineticlimited aggregation, n = 0 indicates irreversible diffusion-controlled gelation. The results are presented in Figure 7D. The slope of $H(\tau)$ at low frequency is similar for phase I and II fibril networks, that is, $n \approx -0.2$. This result suggests that a mixed aggregation mechanism occurs between the kinetic-limited and diffusion-limited regimes with a slight dominance of the latter.³⁵ This conclusion is consistent with the microscopic images shown in Thursch et al., which show regions of percolated fibrils and dense fibril clusters.²⁶ The reformed fibril networks formed after thermal annealing at 50°C show almost identical powerlaw behavior at short times but a much smaller power-law slope at increased time. This is further evidence that the thermal annealing does not produce different gelation processes but only reduces the number of peptides that participate in fibrillization. A lower concentration of peptides leads to slower kinetics, which allow for diffusion-limited aggregation and a more homogeneous percolated network.²⁶

4 | SUMMARY AND CONCLUSIONS

We recently hypothesized that there is a solubility limit of GAG in ethanol/water that induces self-assembly into phase II fibrils. In other

words, above the solubility limit, GAG peptides self-assemble into fibrils until the solubility limit is reached, leaving a soluble fraction in solution. However, it was unknown whether this hypothesis would hold for phase I fibrils. In this study, we determine the effect of temperature on the chemical and mechanical properties of phase I and phase II fibril gels. Chemical properties were probed using FTIR, WAXS, and SAXS. FTIR spectroscopy shows that free peptides are still present in solution after fibril formation, strongly supporting the solubility model. WAXS measurements conclusively show that the phase I and phase II fibrils are composed of almost identical crystalline structures. SAXS was used to show that fibrils are oriented in the network along a preferred axis, which can explain the high packing density that is achieved.

The rheological properties of the fibril networks were probed using SAOS as a function of thermal history. Oscillatory rheology experiments were carried out to determine differences in formation rates and microstructure of phase I and phase II fibril gels. Kinetic traces show that phase I gels form significantly faster than phase II gels before and after annealing, which is attributed to the lower solubility of peptide monomer at lower temperature. Our results clearly show that phase I and phase II fibrils solubilize at $T > 45\,^{\circ}$ C and are equally converted to stable oligomers at high temperatures.

However, the thermal stability of phase II fibrils appears to be higher than phase I fibrils, which at present can only be attributed to differences in helicity. Frequency sweep data clearly show that the conditions of formation and the thermal history mostly impact the gel modulus. For the concentrations studied, the relaxation-time distribution, $H(\tau)$, indicates that all gel phases initially form following a mixed mechanism between kinetic-limited and diffusion-limited aggregation. However, after annealing, phase II fibrils appear to form a more diffusion-limited structure, probably because of the lower concentration of peptides that can form fibrils.

Overall, the effect of temperature seems to support the solubility model proposed previously. The main effect of temperature is to increase the solubility limit of peptide monomer in the ethanol fraction and induce preferential self-assembled fibril helicity. It should be noted that the fibrillization process thus far requires the presence of ethanol, which suggests an organization of the peptides at the water-ethanol interface before fibril formation. One unanswered question is the unexplained transition of peptides at elevated temperatures to stable oligomers that remain soluble at phase I and II formation temperatures. This question is the focus of ongoing studies.

ACKNOWLEDGEMENT

This project is supported by a grant from the National Science Foundation to R.S.S and N.J.A. (DMR-1707770).

ORCID

Nicolas J. Alvarez https://orcid.org/0000-0002-0976-6542

REFERENCES

- 1. Dobson CM. Protein misfolding, evolution and disease. *Trends Biochem Sci.* 1999:24(9):329-332.
- Measey TJ, Schweitzer-Stenner R. Self-assembling alanine-rich peptides of biomedical and biotechnological relevance. Protein Peptide Folding Misfolding Non-Folding. 2012;307-350.
- 3. Murphy RM. Peptide aggregation in neurodegenerative disease. *Annu Rev Biomed Eng.* 2002;4(1):155-174.
- Fichman G, Gazit E. Self-assembly of short peptides to form hydrogels: design of building blocks, physical properties and technological applications. Acta Biomater. 2014;10(4):1671-1682.
- Fukunaga K, Tsutsumi H, Mihara H. Self-assembling peptides as building blocks of functional materials for biomedical applications. *Bull Chem Soc Jpn.* 2019;92(2):391-399.
- Li J, Xing R, Bai S, Yan X. Recent advances of self-assembling peptidebased hydrogels for biomedical applications. *Soft Matter*. 2019;15(8): 1704-1715.
- Panda JJ, Chauhan VS. Short peptide based self-assembled nanostructures: implications in drug delivery and tissue engineering. Polym Chem. 2014;5(15):4418-4436.
- 8. Zhao L, Zou Q, Yan X. Self-assembling peptide-based nanoarchitectonics. *Bull Chem Soc Jpn.* 2019;92(1):70-79.
- Jain R, Roy S. Designing a bioactive scaffold from coassembled collagen-laminin short peptide hydrogels for controlling cell behaviour. RSC Adv. 2019;9(66):38745-38759.
- Szkolar L, Guilbaud JB, Miller AF, Gough JE, Saiani A. Enzymatically triggered peptide hydrogels for 3D cell encapsulation and culture. J Pept Sci. 2014;20(7):578-584.
- 11. Yamada Y, Patel N, Kalen J, Schneider J. Design of a peptide-based electronegative hydrogel for the direct encapsulation, 3D culturing,

- in vivo syringe-based delivery, and long-term tissue engraftment of cells. ACS Appl Mater Interfaces. 2019;11(38):34688-34697.
- Silva GA, Czeisler C, Niece KL, et al. Selective differentiation of neural progenitor cells by high-epitope density nanofibers. Science. 2004; 303(5662):1352-1355.
- Spoerke ED, Anthony SG, Stupp SI. Enzyme directed templating of artificial bone mineral. Adv Mater. 2009;21(4):425-430.
- Altunbas A, Lee SJ, Rajasekaran SA, Schneider JP, Pochan DJ. Encapsulation of curcumin in self-assembling peptide hydrogels as injectable drug delivery vehicles. *Biomaterials*. 2011;32(25):5906-5914.
- Chen C, Zhang Y, Hou Z, Cui X, Zhao Y, Xu H. Rational design of short peptide-based hydrogels with MMP-2 responsiveness for controlled anticancer peptide delivery. *Biomacromolecules*. 2017;18(11): 3563-3571.
- Naskar J, Palui G, Banerjee A. Tetrapeptide-based hydrogels: for encapsulation and slow release of an anticancer drug at physiological pH. J Phys Chem B. 2009;113(35):11787-11792.
- 17. Gazit E. Self assembly of short aromatic peptides into amyloid fibrils and related nanostructures. *Prion*. 2007;1(1):32-35.
- Reches M, Porat Y, Gazit E. Amyloid fibril formation by pentapeptide and tetrapeptide fragments of human calcitonin. *J Biol Chem.* 2002; 277(38):35475-35480.
- DiGuiseppi D, Milorey B, Lewis G, et al. Probing the conformationdependent preferential binding of ethanol to cationic glycylalanylglycine in water/ethanol by vibrational and NMR spectroscopy. J Phys Chem B. 2017;121(23):5744-5758.
- DiGuiseppi D, Schweitzer-Stenner R. Probing conformational propensities of histidine in different protonation states of the unblocked glycyl-histidyl-glycine peptide by vibrational and NMR spectroscopy. J Raman Spectrosc. 2016;47(9):1063-1072.
- DiGuiseppi D, Thursch L, Alvarez NJ, Schweitzer-Stenner R. Exploring the thermal reversibility and tunability of a low molecular weight gelator using vibrational and electronic spectroscopy and rheology. Soft Matter. 2019;15(16):3418-3431.
- DiGuiseppi DM, Thursch L, Alvarez NJ, Schweitzer-Stenner R. Exploring the gel phase cationic glycylalanylglycine in water/ethanol. II. Spectroscopic, kinetic and thermodynamic studies. J Colloid Interface Sci. 2020:573:123-134.
- Farrell S, DiGuiseppi D, Alvarez N, Schweitzer-Stenner R. The interplay of aggregation, fibrillization and gelation of an unexpected low molecular weight gelator: glycylalanylglycine in ethanol/water. Soft Matter. 2016;12(28):6096-6110.
- Hesser ML, Thursch L, Lewis T, DiGuiseppi D, Alvarez NJ, Schweitzer-Stenner R. The tripeptide GHG as an unexpected hydrogelator triggered by imidazole deprotonation. Soft Matter. 2020;16(17): 4110-4114.
- Milorey B, Farrell S, Toal S, Schweitzer-Stenner R. Demixing of water and ethanol causes conformational redistribution and gelation of the cationic GAG tripeptide. *Chem Commun.* 2015;51(92): 16498-16501.
- Thursch LJ, DiGuiseppi D, Lewis TR, Schweitzer-Stenner R, Alvarez NJ. Exploring the gel phase of cationic glycylalanylglycine in ethanol/water. I. Rheology and microscopy studies. J Colloid Interface Sci. 2019;564:499-509.
- 27. Chiti F, Dobson CM. Amyloid formation by globular proteins under native conditions. *Nat Chem Biol.* 2009;5(1):15-22.
- Nelson R, Sawaya MR, Balbirnie M, et al. Structure of the cross-β spine of amyloid-like fibrils. *Nature*. 2005;435(7043):773-778.
- Girardot R, Viguier G, Pérez J, Ounsy M. FOXTROT: a JAVA-based application to reduce and analyse SAXS and WAXS piles of 2D data at synchrotron SOLEIL. Synchrotron Soleil, Saint-Aubin, France, canSAS-VIII. 2015;14–16.
- 30. Heiney PA. www.datasqueezesoftware.com
- 31. Ilawe NV, Schweitzer-Stenner R, DiGuiseppi D, Wong BM. Is a cross- $\beta\text{-sheet}$ structure of low molecular weight peptides necessary for the



- formation of fibrils and peptide hydrogels? Phys Chem Chem Phys. 2018;20(27):18158-18168.
- 32. Measey TJ, Schweitzer-Stenner R. Vibrational circular dichroism as a probe of fibrillogenesis: the origin of the anomalous intensity enhancement of amyloid-like fibrils. J Am Chem Soc. 2011;133(4): 1066-1076.
- Hermans J, Hermans P, Vermaas D, Weidinger A. Quantitative evaluation of orientation in cellulose fibres from the X-ray fibre diagram. Recueil des Travaux Chimiques des Pays-Bas. 1946;65(6): 427-447.
- 34. Bird RB, Armstrong RC, Hassager O. *Dynamics of Polymeric Liquids*. Fluid mechanics. 2nd ed. 1 John Wiley and Sons Inc; 1987.
- 35. Zaccone A, Winter H, Siebenbürger M, Ballauff M. Linking self-assembly, rheology, and gel transition in attractive colloids. *J Rheology*, 2014;58(5):1219-1244.

SUPPORTING INFORMATION

Additional supporting information may be found online in the Supporting Information section at the end of this article.

How to cite this article: Thursch LJ, Lima TA, Schweitzer-Stenner R, Alvarez NJ. The impact of thermal history on the structure of glycylalanylglycine ethanol/water gels. *J Pep Sci.* 2021;27:e3305. https://doi.org/10.1002/psc.3305